# Analysis of Built-Up Areas from Polarimetric Interferometric SAR images

Stéphane Guillaso, L. Ferro-Famil, A. Reigber* and E. Pottier
IETR Institute, The University of Rennes1, UMR CNRS 6164, "*Image Processing and Remote Sensing group*"
"**SA**R **P**olarimetry **H**olography **I**nterferometry **R**adargrammetry Team"
Campus de Beaulieu – Bat 11C – 263 Av Général Leclerc, CS 74205 F-Rennes Cedex, France
*Technische Universität Berlin, Photogrammetrie & Kartographie, Strasse des 17. Juni 135, EB9, D-10623 Berlin, Germany

***Abstract*—This paper describes the analysis of built-up areas using fully polarimetric interferometric SAR data at L-band. This approach uses a polarimetric interferometric segmentation to determine the number of dominant scattering mechanisms required by an interferometric phase estimation using ESPRIT method.**

## I. INTRODUCTION

Over man-made areas, the estimation of the interferometric phase is complex due to highly spatially concentrated scatterers like buildings, houses, vegetated areas, trees, … All these targets introduce multiple scattering mechanisms like isotropic double bounce, cooperative specular reflection, non-cooperative specular reflection, multiple double bounce, rough surface scattering, anisotropic double bounce, and shadow (Fig. 1)

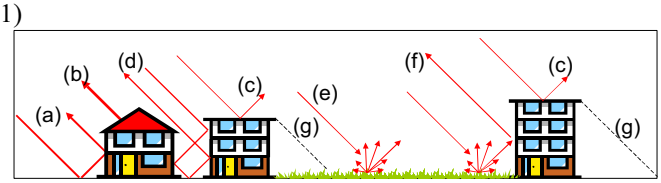


Figure 1. Different scattering mechanisms occurring over build-up areas: (a) isotropic double bounce, (b) cooperative specular reflection, (c) non-cooperative specular reflection, (d) multiple double bounce, (e) rough surface scattering, (f) anisotropic double bounce, and (g) shadow

SAR Interferometry provides a two-dimensional image of elevation angles related to scatterer height. By construction, SAR imaging is a projection of a volume response onto a plane. The retrieval of the scatterer height assumes that only one scattering mechanism occurs in each resolution cell. This assumption is invalid and classical interferometry fails over man-made area. The use of high-resolution methods allows to determine dominant local scatterers and to estimate the corresponding interferometric phases. These methods are based on ESPRIT algorithm, often employed for *direction-of-arrival* (*DoA*) estimation using antenna arrays. For volume areas, like forested terrain, this technique may retrieve the interferometric phase of the ground and the canopy [1]. This approach can be extended over built-up areas in order to estimate the interferometric phase of dominant scattering mechanisms presented in Fig. 1 [2-3].

In part II, some classical interferometry principles are presented, like the height retrieval from the interferometric phase. Part III introduces the ESPRIT algorithm principle applied to fully polarimetric SAR data. In part IV, the efficiency of this polarimetric interferometric approach over built-up areas is shown using fully polarimetric SAR data, obtained from DLR-ESAR airborne sensor in L-band repeat-pass mode.

## II. SAR INTERFEROMETRY (INSAR)

SAR interferometry is an established technique to extract topographic information of a terrain. It is based on the generation of an interferogram between two complex SAR images ($S_1$ and $S_2$) acquired from two slightly different incidence angles. The geometry of an InSAR measurement is represented in Fig. 1. The sensors $A_1$ and $A_2$ are separated by a baseline $B$. A target, $P$, is located on the scene at the height $h$. $R_1$ and $R_2$ represent the distance between sensors $A_1$ and $A_2$ and the target. $\theta$ is the look angle, $\alpha$ is the angle between the baseline, $B$, and the horizontal direction and $H$ is the altitude of the platform. apply

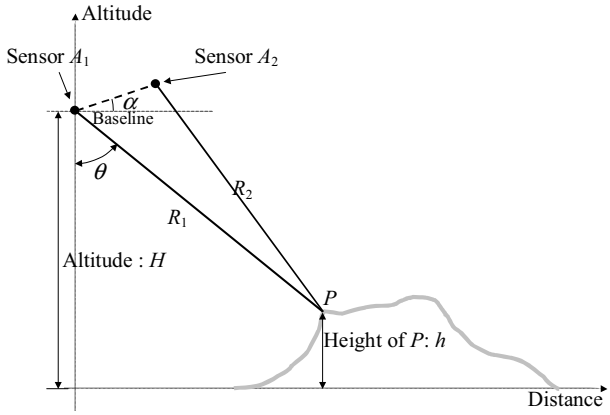


Figure 2. Geometry of an interferometric measurement

The complex interferogram phase, $\Delta\phi$, is obtained by multiplying the first signal by the complex conjugate of the second:

$$\Delta\phi = \arg\left(S_1 \cdot S_2^*\right) = \frac{4\pi}{\lambda}\Delta R = \frac{4\pi}{\lambda}\left(R_1 - R_2\right) \qquad (1)$$

with $-\pi \le \Delta\phi \le \pi$

Using trigonometric relations, (1) may be expressed in terms of the imaging geometry parameters as:

$$\Delta\phi(r) = -\frac{4\pi}{\lambda} B \sin\left(\theta(r) - \alpha\right) \qquad (2)$$

In an airborne configuration, some geometric parameters are range dependant. It is the case for the look angle, $\theta(r)$, and the distance between sensor and target, $R_1(r)$, with $r$ representing the position of the studied point along the range axis.

This phase difference, $\Delta\phi$, contains information about both the range distance and the height of $P$. The information related to the range distance is known as the *flatearth phase*, $\phi_{fe}$. This is the phase difference between two points located at the same reference height ($h_{ref}$) but at different positions in range. The reference height is the altitude at which SAR images are processed.

$$\phi_{fe} = -\frac{4\pi}{\lambda}\frac{B\cos(\theta-\alpha)}{R_1(\theta)\tan\theta} \tag{3}$$

The height related phase information of the studied target, $P$, is the topographic phase, $\phi_{topo}$, which is the difference between the interferometric phase $\Delta\phi$ and the flatearth phase $\phi_{fe}$:

$$\phi_{topo} = \arctan\left(S_1 \cdot S_2^* \cdot \mathrm{e}^{-i\phi_{fe}}\right) \tag{4}$$

$\phi_{topo}$ is directly related to the height variation, $\Delta h$, between the reference height, $h_{ref}$, and the height, $h$, of the point $P$ by the following relation:

$$\Delta h = -\phi_{topo}\frac{\lambda}{4\pi}\frac{R_1(\theta)\sin\theta}{B\cos(\theta-\alpha)} \tag{5}$$

## III. Phase Estimation Using ESPRIT Approach

Backscattered waves result from the sum of contribution corresponding to different scattering mechanisms. Depending on the nature of the observed medium, the value of the resulting interferometric phase may vary in a significant way. The use of the ESPRIT technique permits to separate the different scattering mechanisms and to estimate the main interferometric phase.

The signals acquired during an interferometric measurement, $s_1$ and $s_2$, may be written as:

$$\begin{aligned} s_1^{pq} &= \sum_{m=1}^{d} \sigma_m \zeta_m^{pq} \cdot \mathrm{e}^{i\frac{4\pi}{\lambda}R} + n_1^{pq} \\ s_2^{pq} &= \sum_{m=1}^{d} \sigma'_m \zeta'^{pq}_m \cdot \mathrm{e}^{i\frac{4\pi}{\lambda}(R+\Delta R_m)} + n_2^{pq} \end{aligned} \tag{6}$$

where $pq$ denote the polarization channel (*HH*, *HV*, *VH*, *VV*). These signals consist of a sum of $d$ different elementary scattering contributions represented by $\zeta_m^{pq}$ and $\zeta'^{pq}_m$ denoting the normalised backscattering coefficients of the $m$-th local scatterer in the $pq$ polarisation, and $\sigma_m$ and $\sigma'_m$ denoting the intensity of the $m$-th local scatterer. $R$ is the slant range distance from the master orbit. $\Delta R_m$ is the range difference of the $m$-th scatterer between master and slave tracks. Finally $n_m^{pq}$ denotes additive Gaussian noise in the $pq$ polarization channel. matrix and vector notation, (4) may be written as:

$$\begin{aligned} &\vec{s}_1 = \mathbf{A}\vec{\sigma} + \vec{n}_1 \text{ and } \vec{s}_2 = \mathbf{A}'\vec{\sigma}' + \vec{n}_2 \\ &\text{with } \vec{s}_{1,2} = \left[s_{1,2}^{HH} \quad s_{1,2}^{HV} \quad s_{1,2}^{VH} \quad s_{1,2}^{VV}\right]^T \end{aligned} \tag{7}$$

In the case of sufficiently small baselines, scattering coefficient of each local scatterer for both interferometric acquisitions are assumed to be remain identical: $\zeta_m^{pq} \approx \zeta'^{pq}_m$, $\sigma_m \approx \sigma'_m$. Then, $\vec{s}_2$ may be simplified as follows:

$$\vec{s}_2 \approx \mathbf{A}\Phi\vec{\sigma} + \vec{n}_2 \text{with } \Phi = \mathrm{diag}\left\{\mathrm{e}^{i\phi_1}, \mathrm{e}^{i\phi_2}, \cdots, \mathrm{e}^{i\phi_d}\right\} \tag{8}$$

The form of (5) and (6) are adapted to the TLS-ESPRIT algorithm. Thus, the interferometric phase of each dominant scatterers can be estimated from $\mathbf{\Phi}$.

The TLS-ESPRIT algorithm is based on a covariance matrix formulation, gathering the different scattering coefficients, $\mathbf{R}_{XX}$ defined as:

$$\begin{aligned} &\mathbf{R}_{XX} = \left\langle \vec{k}\vec{k}^{\dagger} \right\rangle \\ &\text{with } \vec{k} = \left[s_1^{HH}, s_1^{HV}, s_1^{VH}, s_1^{VV}, s_2^{HH}, s_2^{HV}, s_2^{VH}, s_2^{VV}\right]^T \end{aligned} \tag{9}$$

the (8×8) matrix, $\mathbf{R}_{XX}$, is then decomposed onto its eigenvector basis as follows:

$$\left\langle \mathbf{R}_{XX} \right\rangle = \mathbf{E}\Lambda\mathbf{E}^{\dagger} = \sum_{m=1}^{8} \lambda_m \vec{e}_m \vec{e}_m^{\dagger} \tag{10}$$

where $\mathbf{\Lambda} = \mathrm{diag}\{\lambda_1,\ldots,\lambda_8\}$, $\lambda_1 \geq \ldots \geq \lambda_8$ and $\mathbf{E} = [\vec{e}_1 | \ldots | \vec{e}_8]$ represent the eigenvalue and eigenvector matrices respectively. The number of dominant local scatterers, $d$, is determined by a polarimetric technique based on an eigenvalue analysis [4] ($d$ is assumed to be inferior to the total number of polarisation channels, in this case, $d \leq 3$).

The eigenvectors corresponding to the $d$ dominant eigenvalues can be decomposed into two ($n \times n$) matrices $\mathbf{E}_X$ and $\mathbf{E}_Y$:

$$\mathbf{E}_S = \left[\sqrt{\lambda_1}\vec{e}_1, \cdots, \sqrt{\lambda_d}\vec{e}_d\right] \begin{matrix} \mathbf{E}_X \\ \mathbf{E}_Y \end{matrix} \tag{11}$$

Applying a second eigendecomposition leads to:

$$\mathbf{E}_{XY}^* \mathbf{E}_{XY} \overset{\text{def}}{=} \begin{matrix} \mathbf{E}_X^{\dagger} \\ \mathbf{E}_Y^{\dagger} \end{matrix} \left[\mathbf{E}_X \quad \mathbf{E}_Y\right] = \mathbf{E}\Lambda\mathbf{E}^{\dagger} \tag{12}$$

$\mathbf{E}$ is partitioned into $d \times d$ submatrices:

$$\mathbf{E} = \begin{matrix} \mathbf{E}_{11} & \mathbf{E}_{12} \\ \mathbf{E}_{21} & \mathbf{E}_{22} \end{matrix} \tag{13}$$

Roy and Kailath [5] show that the eigenvalues $\lambda'_m$, of $\Psi = -\mathbf{E}_{12}\mathbf{E}_{22}^{-1}$, correspond to the diagonal elements of $\mathbf{\Phi}$. Then the interferometric phase of each local scatterer, $\phi_m$, can be estimated by:

$$\phi_m = \arg(\lambda'_m) \tag{14}$$

## IV. BUILDINGS EXTRACTION


Figure 3. Optical image of the Oberpfaffenhofen test site

Fig. 2 shows an optical image of the Oberpfaffenhofen test site. ❶ indicates the building under study. Information given by polarimetric interferometric segmentation are useful to determine the number of mechanisms present in the resolution cell. The ESPRIT algorithm needs an estimation of the number of source to estimate the appropriate interferometric phase.

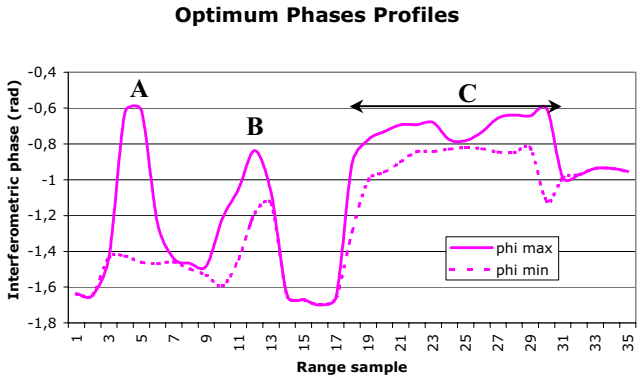


Figure 4. Optimum phase profiles of the understudy building

Fig. 4 shows the optimum phase profiles of the line in Fig. 3. It is obvious that the phases reach a limit (**C** arrow on the graph) which corresponds to the top of the building. **A** and **B** represent the optimum interferometric phase obtained over trees. The behaviour of the two optimum phases permits to discriminate "trees" from "building". Over volume areas, ESPRIT is able to retrieve two different phase terms corresponding to highly different scattering mechanisms. These phase centers indicate scattering over the ground and the tree canopy. Over man-made targets, both phases reach an equivalent value, characteristic of the building top.

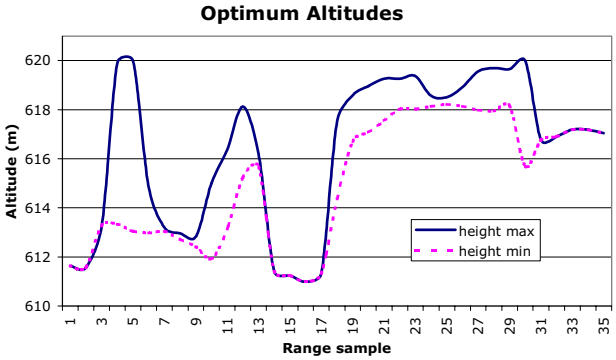


Figure 5. Height profile of the studied building. The measured differenceheight is about 6-7 meters, in accordance with ground truth

From the two optimum phases, the height is calculated using (5). Fig. 5 shows the height profile, of the dashed line in Fig. 3, from the two optimum ESPRIT phases. The difference between the minimum in front of the building and the maximum on its top indicates a height of 6-7 meters, which is in accordance with the ground truth.

## V. CONCLUSION

This paper presents a built-up area analysis using polarimetric interferometric L-band SAR data. The use of high-resolution methods, like the ESPRIT algorithm, is helpful to determine the building height. This approach permits to discrimine the different interferometric phase of dominant scattering mechanisms and provides two optimum phases. These phases may be used to improve the retrieval height accuracy.

## REFERENCES


[1] H. Yamada et al., "Polarimetric SAR Interferometry for Forest analysis based on the ESPRIT algorithm", *IEICE Trans. Electron.*, Vol E84-C, pp 1917-1924, 2001

[2] S. Guillaso, L. Ferro-Famil, A. Reigber, and E. Pottier, "Polarimetric Interferometric SAR Analysis based on ESPRIT/MUSIC methods", *POLINSAR*, Roma, January 2003

[3] S. Guillaso, L. Ferro-Famil, A. Reigber, and E. Pottier, "Urban Area Analysis Based on ESPRIT/MUSIC Methods using Polarimetric Interferometric SAR", *URBAN03*, Berlin, May 2003

[4] L. Ferro-Famil, E. Pottier, and J. S. Lee, "Classification and Interpretation of Polarimetric Interferometric SAR data", IEEE IGARSS'02, Toronto, June 2002

[5] R. Roy and T. Kailath, "ESPRIT – Estimation of Signal Parameters via Rotational Invariance Techniques", *IEEE Trans. Acous. Speech Signal Processing*, Vol. 37, pp. 984-995, 1989